

We are IntechOpen, the world's leading publisher of Open Access books Built by scientists, for scientists

6,900

Open access books available

186,000

International authors and editors

200M

Downloads

Our authors are among the

154

Countries delivered to

TOP 1%

most cited scientists

12.2%

Contributors from top 500 universities



WEB OF SCIENCE™

Selection of our books indexed in the Book Citation Index
in Web of Science™ Core Collection (BKCI)

Interested in publishing with us?
Contact book.department@intechopen.com

Numbers displayed above are based on latest data collected.
For more information visit www.intechopen.com



Application of Powder Metallurgy Methods for Production of a Novel Cu-Based Composite Frictional Train Brake Material

Glenn Kwabena Gyimah, Zhongning Guo,
Ping Huang and Dong Chen

Additional information is available at the end of the chapter

<http://dx.doi.org/10.5772/67533>

Abstract

A novel Cu-based composite frictional train brake material composed of several elements such as Al, SiO₂, Fe, graphite, Sn, Mn and SiO₂ re-enforced with other elements was treated under Powder Metallurgy (P/M) route. The materials were sintered at three different temperatures (850°C, 900°C and 950°C) at a constant pressure.

The tribological behavior of these materials was analyzed by pad-on-disk tests without lubrication and the coefficient of friction, wear rate and wear number were studied in order to identify the effects of the sintering temperature on the base materials composition. The pores in the sintered material were mainly solid lubricants such as graphite and other low melting elements. This resulted in poor hardness and mechanical properties, which were compensated by its ability to reduce seizure.

The wear mechanisms that were generated are as follows; delamination, plowing and abrasive wear. The abrasive wear were dominant and found on samples sintered at 850°C and 900°C, it is seen to be responsible for high wear rates. The friction coefficient under high pressure (3.13MPa) dry conditions had average values of 0.404, 0.343, and 0.336, at 950°C, 900°C and 850°C respectively. The investigation of worn surface was assessed by using x-ray diffractometry and scanned electron microscope.

Keywords: copper matrix, friction material, wear mechanism, train brake pad

1. Introduction

Railways play a major role in world transportation. Providing safety for passengers and property has always been a major concern for train manufacturers and designers. Despite this fact, accidents happen in railroad systems causing casualties and financial losses. There is an

old adage that says, “A train does not have to start, but it must stop.” This presupposes that on a journey, there are changes going on within the tribological system such as the rail-wheels and brake pads/shoes. Materials are worn out and changes in structure occur due to high contact pressures. Also, temperature increase occurs which leads to an altering of mechanical properties and hardness of surface layers. Effective stopping of the train depends on the nature of the worn surface of the pads/shoes. This has been a safety issue, which always attracts additional attention, especially in a time when high-speed trains are the order of the day. The aim of engineering design of friction material is to maximize friction forces, which are the task the system is for, and to minimize wear and tear on complex technical systems. The chemical composition of pads seems to be the major controlling factor for the friction process to build up structured layers in contact zones. Yet the connection between component mixture and friction layer and rate of wear and the connection between friction layer and friction behavior and the rate of wear of the system remains unknown, which makes the entire design complex.

Wear is simply defined as “the progressive loss of substance from the operating surface of a body occurring as a result of relative motion at the surface [1].” The wear requires many changes of pads if the right materials are not used due to excessive and poor wear resistance properties. This becomes an indispensable economic issue. Wear is an applied science. Two common forms of wear are adhesive wear and abrasive wear. Adhesive wear is also known as scouring, galling, or seizing. Deformation in shear is the main mechanism in adhesive wear. During abrasive wear, the surface asperities are worn down and the contact surfaces become mated. Hard ceramic particles like as WC or SiC becoming confined between the sliding surfaces results in abrasive wear. The level of material loss is related to the relative hardness of the ceramic particles and the sliding surface. Another additional factor in wear which can lead to fretting, cavitation, and erosion is environment. Wear is also known as the system property. So variables such as the matrix, reinforcement fibers or particles, orientation of fibers with respect to the wear direction, reinforcement/matrix interface, morphology, and size, and volume fraction of the phases in the composite are all intrinsic microstructural variables and are not currently properly defined. **Figure 1** shows the basic design of the braking system. Disk

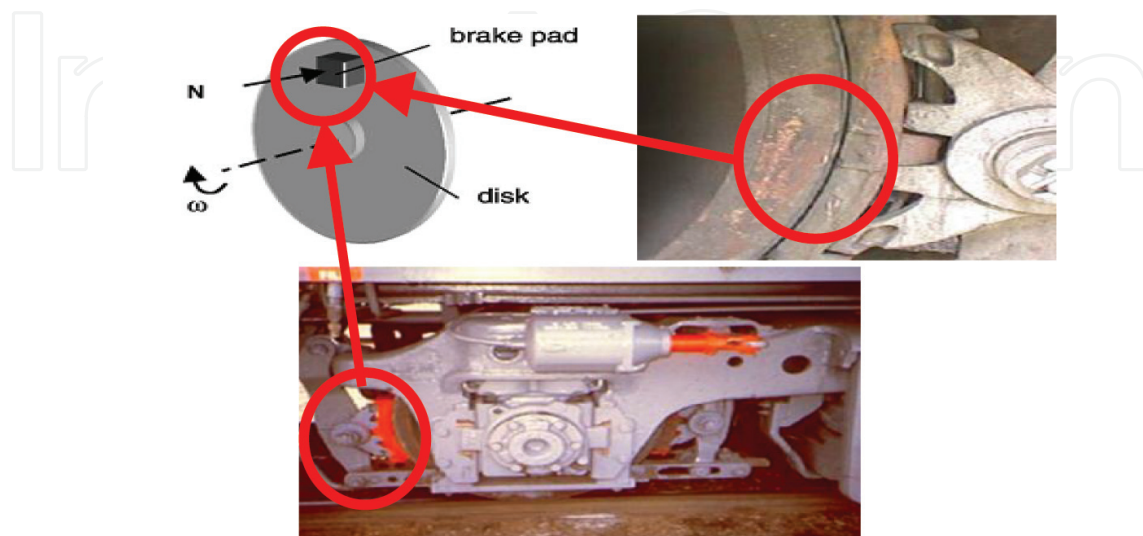


Figure 1. Basic braking system design.

brakes are the most common equipment used to stop vehicles such as cars and trains. This study is based on evaluating the impact of sintering conditions (sintering pressure and temperature) on the mechanical and tribological characteristics of the newly developed Cu-based frictional material for train brake pads. This study also analyzes weight reduction of the rolling stock design with the new material in contrast with old cast iron systems.

The different types of rolling stock have a form-braking device, to the extent that they decelerate and stop when required [2]. A small truck running on rails in mines was the first train car with a braking system. Apparently the mine cars employed a lever to push a wood block against a wheel. Nevertheless, these manual devices became inadequate as the mass and speed of the rolling stock increased. Braking systems using motive power were then introduced. With this in perspective, railway companies began installing braking equipment, usually using either vacuum brakes or air brakes. Only air brakes are currently still being used with the vacuum brakes in abeyance [2].

Compressed air forces piston-driven brake shoes against the wheel in an air-brake system. The composition of the brake shoes can be obtained from a number of different substances, comprising synthetic materials and cast iron. The braking force is not applied directly to the wheel in some contemporary systems. Taking in a disk brake system as an example, the force is applied by clamping brake calipers to both sides of axels-mounted or wheel-mounted disks. This normally helps to consequentially stop the wheel [2]. **Figure 2** shows the cast brake shoes with wear indicators.



Figure 2. The cast brake shoes with wear indicators.

2. Mechanical braking system

The most fundamental and elementary braking devices used by mechanical braking systems are wheel-tread brakes, axle-mounted disk brakes and wheel-mounted disk brakes. The entire mechanisms use an object such as brake shoe or lining that applies friction to the functioning disk. Whenever the applied pressure is adjusted it helps to control the braking force. When the brake shoe applies friction to the wheel threads in the wheel-tread brake, it creates a sliding effect. Since doing so would damage the wheel thread high-speed trains cannot use this type of brake.

Instead they use axle-or wheel-mounted disk brakes. Axle-mounted disks brakes are used on trailer bogies, because they have sufficient space to accommodate such a system. Wheel-mounted disks are dead weight, which are useful only during braking so operators are keen

to install light disks. Carbon/carbon-composite multidisks and aluminum composite disks offer lighter weights and are viewed with considerable interest. A frictional force that slackens the wheel or axles occurs when the carbon/carbon-composite multifiber rotor and stator rub against each other. Comparatively, the disk is lighter than conventional materials and has first-rate heat-resistant qualities. Also, aluminum-composite brake disks could be prepared much lighter than the current forged steel and cast iron brake disks in the market. Additionally, their make-up is the same for both wheel-mounted and axle disks, resulting in a much lighter disk without design alterations.

2.1. Friction materials

The main function of friction brakes is to reduce a vehicle by changing the kinetic energy of the vehicle to heat, through friction, and dissipating that heat. There are two basic types of friction brakes—pad/disk brakes and shoe/drum brakes. Heat flow, reliability, noise characteristics, and ease of maintenance are affected by the designs of the brakes. In this research, we will be looking at the later one.

According to documented historical records, the uses of diverse kinds of materials like friction materials are used for brakes. Wagon brakes used wood and leather are typical examples. A lot of the current brake materials still consist of organic-based materials, like polymers and plant fibers. Incipient railroad IT in the 1800s demanded brake materials to perform under high loads and speeds. According to Nicholson [3], Herbert Froot is credited with discovering the first brake lining material in 1897. This consisted of a cotton-based material saturated with a bitumen solution and was used for wagon wheels as well as primarily designed ancient automobiles. Herbert Froot's discovery paved the way to the initial woven brake lining materials. But in the 1920s crysotile asbestos fibers were used as a substitute. In the 1950s, the common metallic linings were resin-bonded, and the alleged semimets became established by 1960s. These comprise of a higher quantity of metal additives. Common brake materials from Nicholson can be seen in **Table 1** [3].

2.2. Additives and brake materials functionality

Shoe additives and brake pad serve differing functions. Just a slight difference of 2% of additive concentration can have adverse effect on the performance, consequently making composition control vital. The volume percent is most appropriate to list compositions of brake additives, even though many researchers do not adhere to this [3]. Brake materials and additives can be grouped according to their expected functions as shown:

- Abrasives
- Friction modifiers
- Fillers and reinforcements
- Binder materials

Some of the additives can be arranged into more than one category since they fulfill different functions to avoid ambiguity. Subsequently, overlaps of some additives are unavoidable. More so, normally, there are 5–10% of porosity present in the brake materials. The wear

Description of materials	Application(s)	Appro. year
Woven asbestos with brass and other wires for increased strength and performance	Automobiles and trucks	1908
Glass fibers, mineral fibers, metal fibers, carbon and synthetic fibers to provide semi-metallics with higher performance than asbestos (beginning of safety issues with asbestos)	Automotives and trucks	1960s
Dry-mix molded material to replace cast iron brake blocks that produced metallic dust that shorted electric train rails	London underground	ca. 1930
Non-asbestos (fiberglass) materials	Brake drums on original equipment cars	1980s
Cast iron on steel	Railroad car brake blocks and tires	Prior to 1870s
Use of carbon fibers	Automotive brakes	1991
Hair or cotton belting (limited by charring at about 300° F)	Wagon wheels and early automobiles	1897
Molded linings with shorter chrysotile fibers, brass particles, and low-ash bituminous coal	""	1926
Flexible resin binders developed along with more complex formulations	Brake drum linings	1930s
Resin-bonded metallic brake linings	Industrial and aircraft applications	1950s

Table 1. The historical compositions of automotive friction brake materials.

behavior is mostly influenced by size, the form and distribution of the particle of the additive, therefore, investigation must not be limited to only the composition of additives to control friction and wear [3]. Abrasives help maintain the cleanliness of mating surfaces and control the build-up of friction films. They also increase friction, particularly when initiating a stop. These materials lubricate, raise the friction, or react with oxygen to help control interfacial films. Fillers are used to maintain the overall composition of the friction material and some have other functions as well. They can be metals, alloys, ceramics, or organic materials. Commonly known to have the capability to absorb heat generated by friction as the same time ensuring the efficiency of the brake system is cashew frictional dust. This is in a granular form. It produces a softer material at higher efficiency for wear when the brakes are relatively cold. This benefit outplays plain phenolic resin. Cardanol is the primary constituent in cashew nutshell liquid and is hydrophobic and remains liquid and flexible at very low temperatures. The popular and original binder materials are phenolic resins in the case of automotive and truck pads. In the case of aircraft, there are three basic types of aircraft friction brake materials: (1) sintered metal, (2) carbon-carbon, and (3) organic materials. But the Cu-based matrix materials tend to have a higher friction response than Fe-based metallic [4]. Asbestos is also known as hydrated magnesium silicate $Mg_3Si_2O_5(OH)_4$. The content of asbestos in vehicle brakes varies between about 30–70% when it is used. The admirable properties of asbestos include accessibility at reasonable cost, insulate thermally, and stable at 500°C and above. This produces silicates, aid to regenerate the friction surface during use, flexible yet strong nature, produces harder and abrasive silicates, well processed, and wears well. It is able to maintain its fibrous property until about 1400°C, and at higher temperature, it becomes dehydroxylated [5]. The variation in cost, processing, and properties are a factor

to determine the type of asbestos to be used. Amosite and crocidolite are other asbestos minerals that are used even though chrysotile is normally available too. Actinolite, anthophyllite, and tremolite are the other types, which are not so famous and found mainly as minor impurities together with other minerals.

2.3. Typical compositions and designations of brake friction

All friction coefficients for brake material pairs have a range of 0.07–0.7, but practically, most vehicles operate within a narrower range according to Ref. [6]. Actual standards range from about 0.3 to 0.6 in friction coefficient. The frictional materials are classified into six categories, which are dependent upon operational capabilities. The operation conditions are influenced by the class number as higher class number requires severe operating conditions. Materials must be designed to withstand the energy dissipation demands of the usage. The class numbers goes with the pressure, temperature, and speeds for the operating condition [6]. Some of the most challenging issues facing the engineer are basically to understand the degradation processes known as wear, to predict the rate of wear, and to reduce it. The appreciation of wear often involves a comprehensive knowledge of mechanics, physics, chemistry, and material science, while its quantitative prediction, even to within an order of magnitude, remains in many cases a distance goal [7]. The broad definition of wear includes the loss of material, movement of material within a single surface, or transfer of material from one surface to another [8]. It is alleged that [9] the loss of substance form the operating body in a progressive order. This is as a result of the relative motion of the wear. But a comprehensive definition covering extensive range of engineering applications such as tribologist is appropriate. A damage to the body surface is a valuable account to wear, which involves progressive loss of material as a result of relative motion between the contacting bodies [10]. The mechanisms of degradation are not considered in these definitions. These may be solely mechanical, involving plastics deformation or brittle fracture, having chemical aspects. Both chemical and mechanical methods play a role in many practical cases [11].

The arrangement and grouping of wear parameters, along with descriptive terms of the wear mechanisms such as impact wear, sliding wear, rolling wear, and fretting wear are used in literature and in practice. These are used to describe the motion that occurs in wear. Nevertheless, wear mechanisms, which are mechanical, thermal, and chemical wear, are not described. Wear administered solely by the processes of deformation and fracturing are basically described by mechanical wear. For brittle materials, the deformation procedure plays a major role in its wear mechanism [12–14]. The tribochemical wear describes the wear governed by chemical and thermal. The melting is basically due to friction [15]. Other thermal wear on brittle materials are diffusive wear at elevated temperatures and fracture induced following thermal shocks [16]. These are more expressive terms for mechanical wear. The three-dimensional wear models of surface scratching by a hard asperity have already been suggested and ratified through quantitative agreements between experimental results and theoretical predictions [17, 18]. The wear volume, V , is given by the following formula:

$$V = \frac{\alpha\beta WL}{H_v} \quad (1)$$

where β represents the degree of wear by abrasive asperity, α the shape factor of an asperity, L the sliding distance, and W is the load. In practice, 0.1 is used for α and β , which range from 0 to 1.0, based on the depth of penetration of the abrasive particle, mechanical properties of the wearing part, and shear strength between the contact parts. If w_s is the specific wear rate as = wear volume/sliding distance \times load, or K is the wear coefficient as = $w_s H_v$, H_v is the hardness, they are derived from Eq. (1) as follows:

$$K = \beta\alpha \quad (2)$$

$$W_s = \frac{\alpha\beta}{H_v} \quad (3)$$

These formulae are valid for only single-abrasive scratching.

As for the adhesive wear of ductile materials, no prognostic theories have been quantitatively confirmed by experimental purposes. Even though the suppositions of wear particles are removed based on unit contact, it still did not agree well with experimental data to provide a basis for a quantitative theory [19, 20]. The adhesive wear equations which are comparable to the equation are expressed as follows, Eq. (1):

$$V = w_s WL \quad (4)$$

$$V = \frac{KWL}{H_v} \quad (5)$$

Experimental results for the adhesive wear show that the wear volume increases almost linearly with the load and sliding distance. However, useful physical models were not found to explain the observed variation in values of w_s , and K , where w_s varied from 10^{-2} to 10^{-10} $\text{mm}^3 \text{N m}^{-1}$. Ratcheting is the flow wear, which supposes that experimental analysis agree well to the theoretical model [21, 22].

Fatigue wear estimates high-cycle fatigue, crack initiation, and propagation in a repeated contact stress cycles is dominate. The path of crack propagation decided the size of the wear asperities and its volume per unit. N_f is the critical number of rolling cycles for surface spalling caused by high-cycle fatigue fracture and is experimentally specified by the equation:

$$N_f = bW^{-n} \quad (6)$$

where b and n are constant values for the experiment and W is load. The n value is 3 for ball bearings [23]. It could be analyzed statistically by following the Weibull theory [24]. For low-cycle fatigue wear the Coffin-Manson-type relation can be employed. The theoretical wear rate model in a two-dimensional model is expressed as the plastic wave formation [25]. The K , wear coefficient, is expressed as

$$K = \frac{9 \times 3^{1/2} r \mu}{C^D \gamma_t^{1-D}} \quad (7)$$

where C is the monotonic effective shear strain; r , μ , and γ_t are all determined from the wave model as functions of the attack angle and the normalized shear strength of the contact

interface; and D is an experimental constant used as the power in the low-cycle fatigue law. When strain is accrued to a critical value causing fracture wear is the resulting incident.

2.4. Brake and materials

The purpose of friction brakes is to slow down a vehicle by converting the kinetic energy of the vehicle to heat, by the process of friction and then dissipating that heat. As a part of an automobile, brake materials have additional requirements such as resistance to corrosion, they need light weight, long life, low noise, stable friction, low wear rate, and tolerable cost at good performance. Shoe materials and brake pads and additives and serve a variety of functions. They help survey and improve the requirements of the pad. Even a difference of a percent or two of additive concentration can affect performance in an either negative or positive way, so composition control is crucial.

First of all, the choice of frictional brake materials used depends on several factors. Fundamentally, the properties of the materials are usually the first things to be considered but other factors, such as availability of the material, ease of manufacturing process, and cost, also play important roles. Among the properties that need to be considered are physical properties, chemical properties and mechanical properties. But in this piece of work, the properties are grouped under mechanical and tribological characteristics of the frictional material, of which the composition formation is very important. Powder metallurgy sintered metal friction materials have been used as brake disks, especially for heavy-duty applications. Because of their high performance and low wear rate under high temperatures and heavy-duty conditions, sintered friction materials have become increasingly important. Friction materials are the composites made up of sinterable metal matrixes (e.g., copper and iron), function components or modifiers (e.g., alumina, silica, and mullite), and solid lubricants (e.g., graphite and molybdenum disulfide). Comparatively, Cu-based materials are chosen above other competitors such as Fe-based and Cu-Fe-based materials because of its outstanding advantages. Cu-based materials have demonstrated better heat conductivity and friction resistance, so they are broadly used in aircrafts, trains, automobiles, and shipping brake systems.

Also, copper-based sintered composites produced by powder metallurgy processes are now widely used in industrial applications because of their high thermal conductivity, easy manufacturing, and corrosion resistance. But copper also presents limitations such as low hardness, low tensile yield strength, and poor creep resistance. But these can be overcome by integrating other elements and additives. These elements and additives improve their functions, quality, and performance in engineering applications.

2.5. Methods: powder production techniques

Using a simple powder metallurgy (P/M) route for manufacture, the material is based on the concept of combined properties of a copper-based alloy matrix for good thermal conduction and for good wear resistance performance.

The methodology used here is based on newly prepared sample materials listed in **Table 3** with different compositions of each material. These are subjected to a common constant sintering pressure but with three different sintering temperatures. These will then undergo various kinds of mechanical and tribological behavior tests before and after a thorough brake wear test to verify the rate of material loss which will help determine the wear ability of materials. The results will be mathematically analyzed to give a vivid conclusion about the results of the experiment. See **Figure 3** for the route.

Ingt: Cu	Matrix component (SiO ₂ , Fe & etc.)	Frictional component (Graphite & MoS ₂)	Lubricant element (Mn, Sn & etc.)	Alloying
Wt%.	50–60	15–20	15–20	5.0

Table 2. Chemical compositions of material in mass (wt. %).

Rule of mixture (ROM)	
ρ_i (g.cm ⁻³)	7.973 g.cm ⁻³
Experimental data	
Average ρ (g.cm ⁻³)	6.7136 g.cm ⁻³
Average microhardness (HV)	294
Average porosity %, $P = \left(1 - \frac{\rho}{\rho_i}\right) \times 100$	15.79%

Table 3. Physical properties of cu-based composite.

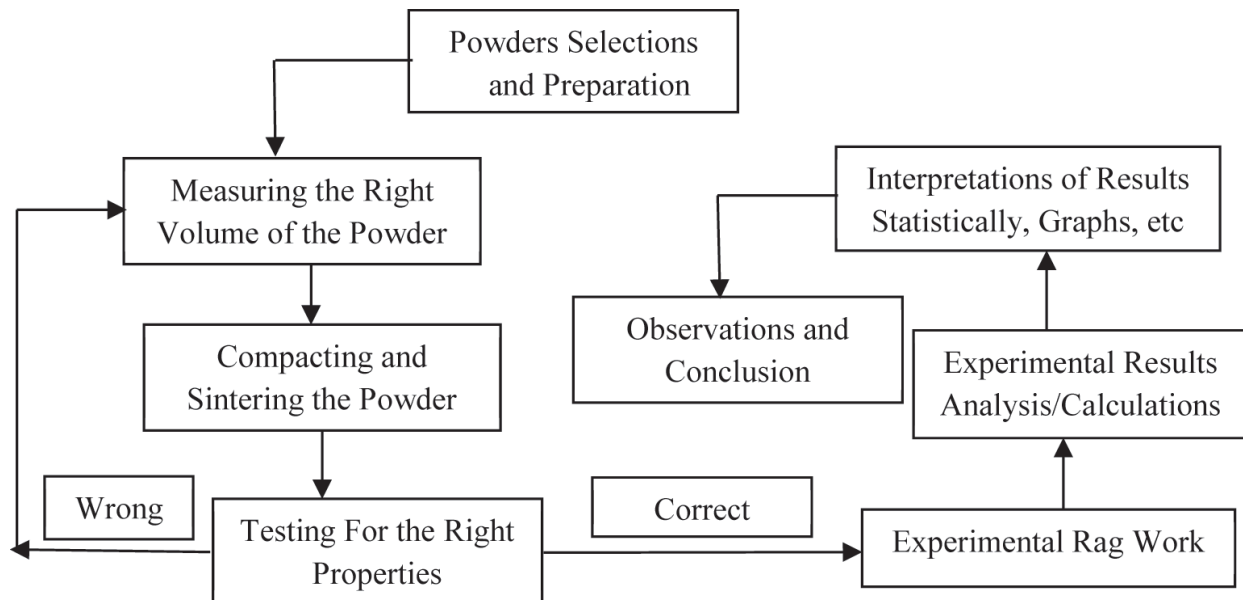


Figure 3. P/M route and experimental method schematic diagram.

2.6. Design of sample, mold, and sample holder

Design of a product is an inventive event whose primary work is to establish the multifaceted properties of objects, processes, services, and their systems in whole life cycles. This makes design a central factor of state-of-the-art humanization of technologies and a very crucial factor of cultural and economic exchange. This design is concerned about how to discover and assess elements, constituents' organization, and functional expressions at three different sintering temperatures, with the following objectives:

- Reducing wear rate of brake pad materials.
- Reducing high frequency of changing brake pads.
- Reducing heavy weight of rolling stock due to the weight of brake pad material compositions (cast iron) within braking systems.
- Improve tribological characteristics of Cu-based alloys for more functions.
- Giving Cu-based frictional products a more effective face and chance to improve upon it products.

Figures 4 and 5 show “die and two steel punches,” a typical rectangular tool. This design was completed according to the ASTM B331-95. The die is made of tool steel and is a rectangular compact. The compacts are made up of the die and the punches, the die is in two layers, the inner layer and the outer layer. The inner layer is made up of high tool steel and the outer layer is made up of mild steel. The punches are also made of tool steel. The rectangular section was chosen because of the type of test rag that was used.

The rectangular blocks were obtained from this mould, which was sintered and then cut and grounded into 14 mm square of the thickness of 6.5 mm. This then gave us 196 mm² per piece, so that the double specimen will then be 392 mm². This is about 31% of the Chinese standard for 0.98 MPa constant pressure friction tester contact area of 25 mm square specimen. This was carried out since the material under consideration was meant to face higher pressure in the railway than the 0.98 MPa as the standard for automobile friction brake materials. The specimen holder was

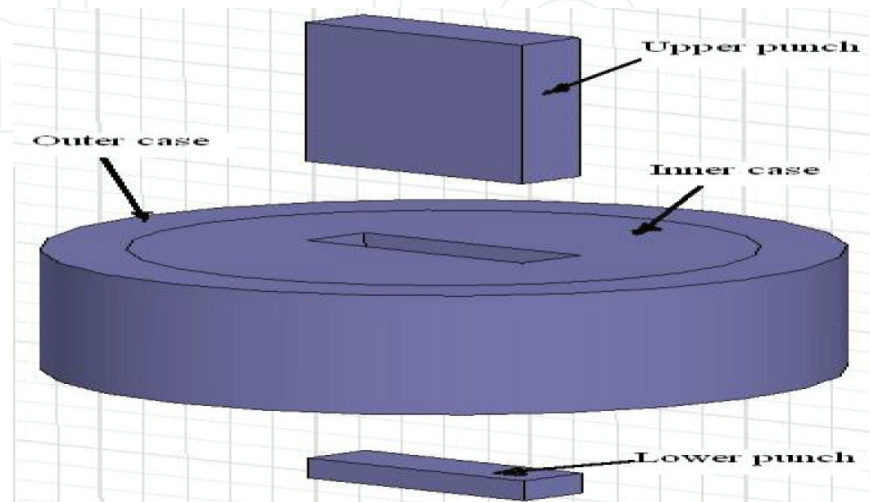


Figure 4. Die and two steel punches.

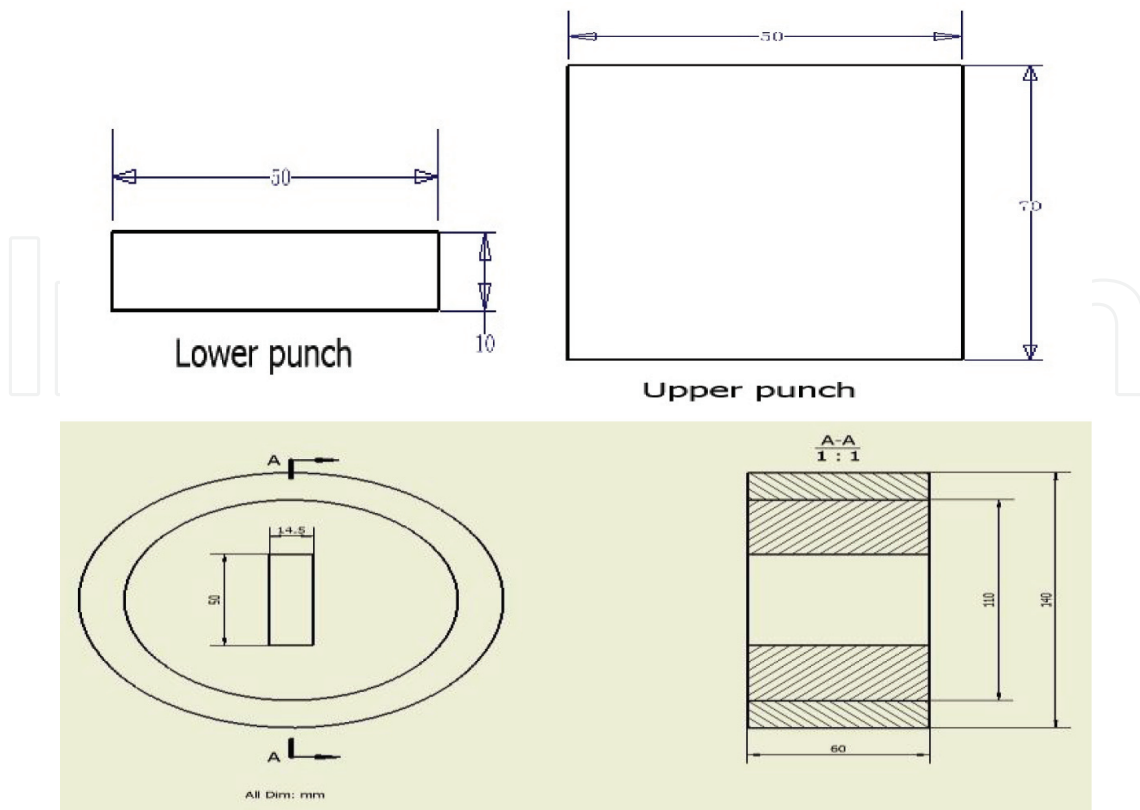


Figure 5. Cross-section of dies and punches.

originally 25×25 mm but due to the need for increased pressure, redesign of the holder was made. A 25×25 mm new holder was designed and produced. Within it was a square space of about 3.5 mm deep and was meant to accommodate a specimen of 14×14 mm. **Figure 6** shows a typical specimen holder. The material used to produce the specimen holder is from #45 steel.

2.7. Sample preparation

The first step was the selection of powder materials categorized under based metal on the matrix, frictional component, lubricant, and alloying element as shown in **Figure 7**. A dry, bulk solid consisting of a big number of very fine specks that may flow freely when shaken or tilted

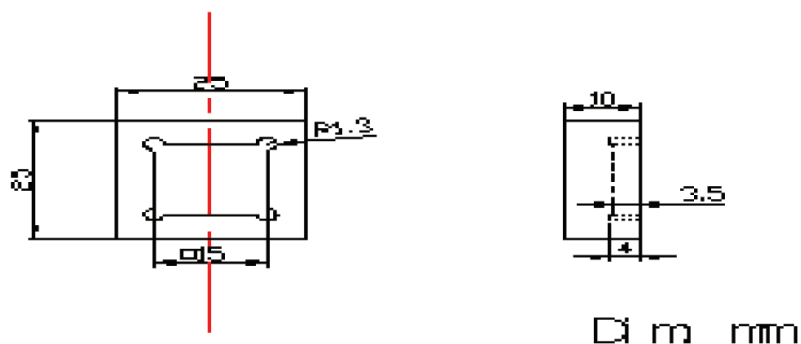


Figure 6. Elevation of the specimen holder.



Figure 7. Powders.

is termed as a powder. They are special subclass of granular materials, even though the terms powder and granular are occasionally used to differentiate separate classes of material. These were centered on the outcome of Kryachek [26] review and Yao et al. [27]. The newly developed bronze-based brake pad powder material with its chemical composition is given in **Table 2**.

The powders listed in **Table 3** were weighed in a sartorius BS224 S (Max 220g d = 0.0001 g) with their given proportion, the well-prepared powder was mixed in a V-cone mixer or double cone mixture machine (**Figure 8** is a mixing machine). The rotating speed of the double cone mixture was maintained at 150 rpm for 9 hours.

In the powder pressing process, the isostatic powder compaction press is employed with tools and dies. The die cavity that is closed on one end (vertical die, bottom end closed by a punch tool) is filled with powder that is subjected to isostatic, which is uniform in all directions, external pressure. As the pressure is isostatic, the as-pressed component is of uniform density. The powder is then in shape and then ejected from the die cavity. The compacting were done in a hardened steel die using a cold (or room-temperature) isostatic pressing hydraulic machine (SANS DCS-300 Digital hydraulic compacting machine) under the pressure of 650 MPa and is shown in **Figure 9**. The isostatic technique is only normally used for semifabricated products such as bars, billets, sheet, and roughly shaped components, all of which require considerable secondary operations to produce the final, accurately dimensioned component.



Figure 8. Mixing machine.



Figure 9. Isostatic compacting machine.

The process of taking metal in the form of a powder and transferring it into a mold or die is called the solid state sintering. As soon as it is compressed into the mold, the material is placed under high heat for a lengthy period of time. This heat treatment equipment is called a furnace is shown in **Figure 10**. Under heat, bonding takes place between the porous aggregate particles. When it is cooled, the powder is bonded to form a solid piece. Sintering can be considered to be made of three stages that are as follows:

1. Neck growth proceeds rapidly but powder particles remain discrete.
2. Most densification occurs, the structure recrystallizes and particles diffuse into each other.
3. The last stage, isolated pores tend to become spheroidal and densification continues at a much lower rate.

The compacts were subsequently transferred into a mesh belt continuous resistance furnace for sintering, shown in **Figure 10**. The sintering took 90 min in a controlled atmosphere furnace saturated with carbon at 850–950°C at 0.01 MPa constant pressure. In order to control the level of porosity, the component is dipped into hot oil for a few hours. The pores were then filled with oil. Finally, the resulting rectangular bar with a thickness of 5 mm was cut and grounded to a size of 14 × 14 mm test specimens. Nine pairs of specimens were prepared for the friction and wear test.



Figure 10. Mesh belt continuous resistance furnaces.

2.8. Testing procedures

The density values of the brake pad materials' were calculated by Archimedean principle, prior to sintering and after. The sample hardness was determined after the sintering process was done by a Digital Micro hardness tester HVS-1000 instrument. The values were taken under 10 N within 30 s. The sand paper grits 1200, 1000, 800, 600, 320, 240, and 180 were used to polish it after grinding. Alcohol was also used in the ultrasonic cleaner to clean all the samples. The micrograph structure investigation was done by scanning electron microscope (SEM) and the optical microscope (OM) prior to the wear test and after. The following two polishing stages of 3 and 0.05 μm , respectively, were done to enable access to the porosity, the microstructure, and the worn surfaces of the newly developed substance [28]. In addition, the energy dispersive spectroscopy (EDS) and the X-ray diffraction (XRD) were also used to observe elements composition and tribosurfaces of the worn surfaces after the wear test to determine the wear mechanism. TALYSURF CLI 1000 was also used to classify the kind of abrasive surfaces observed. **Figure 11** shows the Talysurf CLI 1000.

During the tribotests, the performance tests, which include the calculation of wear loss, frictional coefficient, friction force and a kind of wear, were executed. The parameters in this research were verified in accordance to GB5763-1998 of China National Standard. The friction material tester (X-MSM Constant Speed) of the speed 7.54 ms^{-1} at a constant pressure of 3.13 MPa used with a rotor of Brinell hardness in the range of 196, made of cast iron disk of the grade HTA5/HB. The main units of the test rig were made up of sample tool holder, disk and the control and monitoring unit. The temperatures for the friction test were 350, 300, 250, 200, and 150°C . A pair of different samples was in contact with the gray cast iron disk under a load. The total contact area was about 3.92 cm^2 and rotated at the constant speed of 7.54 ms^{-1} for 5000 revolutions [28]. **Figure 12** shows the tester and the monitor/control unit.

The initial design of the machine suits 0.98 MPa and $25 \times 25 \text{ mm}$ of contact area. The specimen holder was redesigned to cover the contact area of $14 \times 14 \text{ mm}$, as a result of that, pressure



Figure 11. TALYSURF CLI 1000 equipment.



Figure 12. X-MSM constant speed friction material tester and monitor/control unit.

increased to 3.13 MPa on the tested sample. The friction coefficient data were obtained automatically from the tester. The sample pairs that were tested were five each and an average result was taken. Because there is no program to automatically obtain the wear loss directly, volume wear rate V in $\text{mm}^3 \text{N}^{-1} \text{m}^{-1}$ was computed manually after 5000 revolutions of the disk based on pad-on-disk wear testing of ASTM G99-95a. In an unlubricated tribological application under the operating conditions of F_a load, v speed, T temperature, t operating duration, and s sliding distance, friction and wear will occur and must satisfy these standards below [25]:

$$\text{wear coefficient} = \frac{\text{wear volume}}{\text{load} \times \text{sliding distance}} \quad (8)$$

$$k = \frac{W_v}{F_a s} < 10^{-6} \text{mm}^3 \text{N}^{-1} \text{m}^{-1}$$

$$\text{friction coefficient} = \frac{\text{friction force}}{\text{normal load}} \quad (9)$$

$$\mu = \frac{F_F}{F_a} < 0.2$$

$$k = \frac{1}{2\pi R n} \times \frac{\text{volume change}}{\text{average force, } f_a}, \text{ the volume change is } A(d_1 - d_2) \quad (10)$$

where n is the number of rotations of the disk during testing (5000 rev), R is the distance from the middle of the rotating disk to the middle of the specimen ($=0.15 \text{ m}$), A is the area of the specimen (196 mm^2), d_1 is the average thickness of the specimen before the experiment (mm), d_2 is the average thickness of specimen after the experiment (mm), and f_a is the average force of sliding friction (N). They were obtained at temperatures of 100, 150, 200, 250, 300, and 350°C , respectively. The diagrammatical illustration of the tribotester is shown in **Figure 13**.

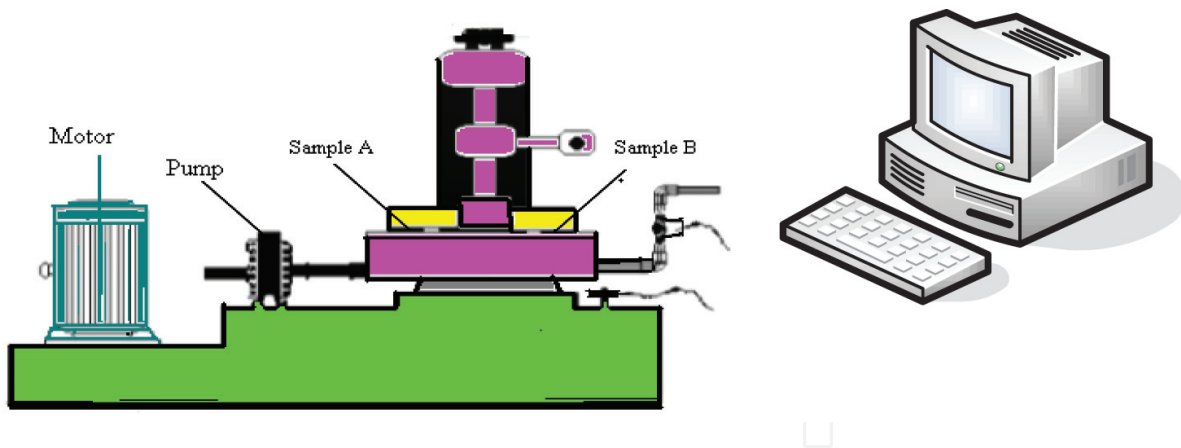


Figure 13. The diagrammatical illustration of the tribotester.

The wear numbers procedure was employed as a way of deciphering the wear resistance level of the specimen. The specimen mass was determined before and after the wear test to calculate the mass lost after 5000 revolutions, at the following temperatures; 350, 300, 250, 200, 150, and 100°C. This was done and the wear number was obtained as:

$$\text{Wear number}(W_n) = \frac{\text{Density}}{\text{Mass loss}} \quad (11)$$

where W_n in revolutions per unit volume of the sample is the wear number. The higher the wear number, the more effective the wear resistance of the material (ASTM B611). The wear numbers obtained are presented in **Table 5**.

It is necessary to examine the structural elements and defects that influence the tribological properties of the materials. Microstructure, which basically refers to the grain size and the shape and other microstructural characteristics, goes a long way in influencing the mechanical and wear behavior of a material. Optical, electron, and scanning probe microscopes are commonly used in microscopy. These instruments aid the examinations of the microstructural features of all types of materials. Microscope investigation is a very important method in the characterization and study of materials. The microstructure and tribosurfaces analysis was done with optical micrograph (OM), the scanning electronic microscope (SEM), energy dispersive spectroscopy (EDS), and X-ray diffraction (XRD). OM and the SEM help analyze the nature of microstructures and pores that are produced. This was done both before and after the wear test. The EDS and the XRD were also used to observe the tribosurfaces of the worn surfaces of the test sample after wear test. The density of friction materials is determined according to the procedure proposed in ASTM D792, which is based on Archimedes' principle. The pressure under which the powder was compacted greatly influences the density obtained. The Cu-based brake pad material was

Sintering temperature, °C	Hv	Density, $q(\text{g.cm}^{-3})$	Porosity, p(%)
850	272	4.504	17.53
900	287	4.645	15.82
950	304	4.843	14.04

Table 4. Mechanical properties of the novel Cu-based friction material.

T_{sin} °C	Disk temperature (T_{disc})					
	100°C	150°C	200°C	250°C	300°C	350°C
850°C						
W_n	8.915	8.446	8.086	7.789	7.224	6.350
k^*	1.428	1.520	1.540	1.560	1.580	1.600
μ	0.394	0.352	0.331	0.324	0.313	0.301
900°C						
W_n	11.16	10.02	9.305	10.62	8.757	9.605
k^*	1.595	1.610	1.630	1.680	1.700	1.720
μ	0.398	0.351	0.341	0.332	0.319	0.317
950°C						
W_n	12.21	11.30	10.44	10.68	8.154	8.874
k^*	0.328	0.409	0.460	0.471	0.490	0.502
μ	0.421	0.412	0.401	0.398	0.397	0.395

NB: k^* , $\times 10^{-4} \text{mm}^3 \text{N}^{-1} \text{m}^{-1}$; W_n , rev/cm^3 [30].

Table 5. Properties of novel material at different T_{sin} and T_{disk} .

used on a rotor, the disk made of cast iron (grade HTA5/HB with Brinell hardness in the range 196). This fulfills the China National Standard GB5763-1998.

All tests were carried out strictly under laboratory environment and experimental standards observed. In the experiments, the speed was constantly rotating at 480 rpm (sliding velocities of 7.54ms^{-1}); constant pressure is 3.13 MPa instead of the original 1 MPa due to the modification of the specimen holder, which eventually reduces the area of the specimen. The load used is 1226 N; the area is reduced to 196mm^2 ($14 \times 14 \text{mm}$). Therefore, the pressure exerted on the sample is $P = F/A$ (MPa). The average of the experimental data of five sample pairs were taken and tested for each specimen. The volume wear rate V in $\text{mm}^3 \text{N}^{-1} \text{m}^{-1}$ was calculated after 5000 revolutions of the disk.

3. Experimental results analysis

3.1. Temperature effect on mechanical behaviors

Strength and ductility, or brittleness, are properties affected by the temperature of operating conditions or manufacturing conditions. Manufacturing conditions affect the mechanical behavior of the material. This impacts performance, safety and economic issues. This experiment considered different heat treatment temperatures within the same composition of the material. The experiment focuses on the effect of the sintering temperature on the following: (a) density and porosity and (b) hardness of the material. To what extent does sintering temperature influence the rate of wear through density, porosity, and hardness?

The role of pores in limiting the mechanical properties of materials is very obvious. They act as areas for initiation of fracture and provide an easy path for crack propagation. The voids, serve as sites of weakness at which ductile fractures may initiate during plastic deformation. This also leads to volume change, eventually affecting the density. In contrast, the voids at certain percentages are also very needful to facilitate self-lubricating properties in dry sliding conditions. This is known in simple terms as porosity, and is defined as the total volume occupied by pores per unit volume of material and is calculated from real density and viewed density. The formula is:

$$\text{Porosity, } P = \left(\frac{\text{Real density} - \text{Viewed density}}{\text{Real density}} \right) \quad (12)$$

$$P = 1 - \left(\frac{\rho_v}{\rho_r} \right) \quad (13)$$

where ρ_r is the real density and ρ_v is the viewed density, in this case calculated to be 7.973 g cm^{-3} by the use of ROM. **Figure 14(a)** and **(b)** shows both the theoretical and the practical outcome of the experiment density and porosity, respectively. This shows the relationship between varied temperatures and properties (density and porosity). Measurements of the density and porosity were carried out according to the standard of the sintered samples [29] and the Archimedes principle. According to the Archimedes principle, mass density of an object is defined as:

$$\rho = m/V \quad (14)$$

where ρ is the mass density of the object, m is the mass of the object, and V is the volume of the object. The principle also asserts that, there is an upward force applied on the object by the fluid known as the buoyant force defined as:

$$F_B = g\rho_F V \quad (15)$$

where g is the acceleration due to gravity, F_B is the buoyant force on the object, V is the volume of the object immersed in a fluid, and ρ_F is the density of the fluid.

According to the Archimedes principle, it is possible to determine the density of an object without ever determining its volume.

$$F_B = W_A - W_F \quad (16)$$

where F_B is the buoyant force on the object, W_A is the normal weight of the object measured in air ($W_A = mg$), and W_F is the weight taken while the object is immersed in a fluid of density ρ_F .

Now, comparing Eqs. (15) and (16), the following was deduced:

$$g\rho_F V = W_A - W_F \quad (17)$$

Solving this equation for the volume of the object, the equation is as follows:

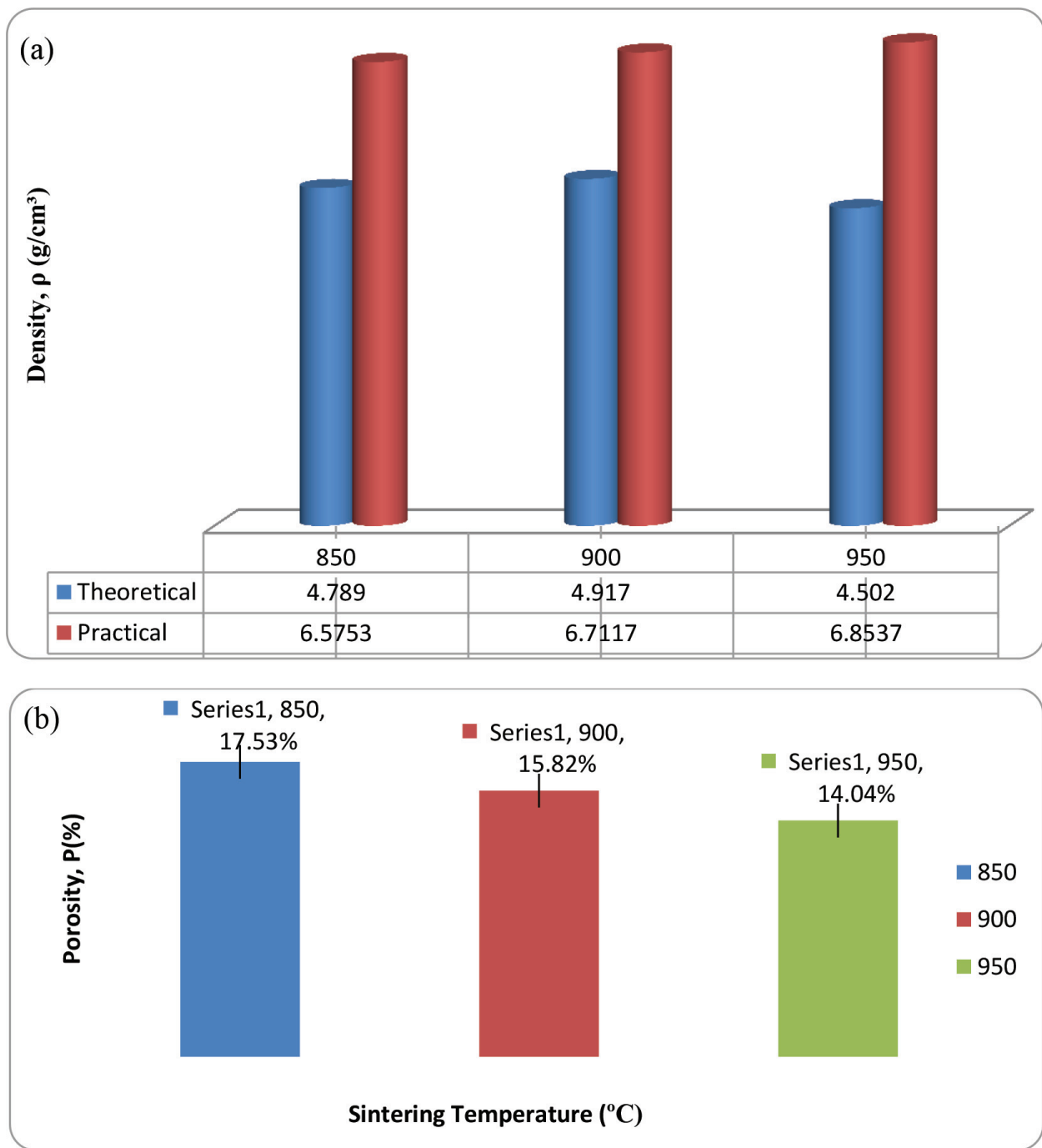


Figure 14. (a) Relationship between density and sintering temperature. (b) Relationship between porosity and sintering temperature.

$$V = (W_A - W_F)/(g\rho_F) \quad (18)$$

and substituting it into the definition of density in Eq. (14) will be (after some simplification) as shown:

$$\rho = \left(\frac{W_A}{W_A - W_F} \right) \rho_F \quad (19)$$

The rules of mixture (ROM) for composite materials were also used and the results were compared with the Archimedes principle. ROM are mathematical expressions, which give some property of the composite in terms of its properties, quantity, and arrangement of its constituents. For density, a general composite, total volume V , containing masses of constituents M_a, M_b, M_c, \dots , the composite density is

$$\rho = \frac{M_a + M_b + M_c + \dots}{V} = \frac{M_a}{V} + \frac{M_b}{V} + \dots \quad (20)$$

In terms of the densities and volumes of the constituents:

$$\rho = \frac{v_a \rho_a}{V} + \frac{v_b \rho_b}{V} + \frac{v_c \rho_c}{V} + \dots \quad (21)$$

But $v_a/V = V_a$ is the volume fraction of the constituent a, hence:

$$\rho = V_a \rho_a + V_b \rho_b + V_c \rho_c + \dots \quad (22)$$

For the special case of a fiber-reinforced matrix:

$$\rho = V_f \rho_f + V_m \rho_m = V_f \rho_f + (1 - V_f) \rho_m = V_f (\rho_f - \rho_m) + \rho_m \quad (23)$$

where ρ the theoretical density of the composite, V is volume fraction of the component, and the subscripts f and m refer to the fiber and matrix, respectively. It is noted that:

$$V_f + V_m = 1 \quad (24)$$

Table 3 shows the physical properties of the novel Cu-based material. The results indicate an increase of more than 5% in density and little decrease in the interconnected porosity. This all occurred at a high sintering temperature (950°C). At other subsequent temperatures (900 and 850°C), the results were not appreciating since it seemed the temperature was not sufficient for the treatment.

Hardness is not an intrinsic material property dictated by precise definitions in terms of fundamental units of mass, length and time. A hardness property value is the result of a defined measurement procedure. Hardness is an indicator of a metal's resistance to plastic deformation (e.g., a small dent or scratch) and it is an important factor that influences the rate of wear of a material. Therefore, the Vickers hardness test was performed on specimens using Digital microhardness tester HVS-1000 instrument according to the ASTM E 8-04 Standard [2]. The term "microhardness test" usually refers to static indentations made with loads not exceeding 1 kgf. The indenter is either the Vickers diamond pyramid or the Knoop elongated diamond pyramid.

The method for analysis and testing is comparable to that of the standard Vickers hardness test. The only difference is that it is accomplished on a microscopic scale with higher precision instruments. The surface being tested commonly demands a metallographic finish. The smaller the load used, the higher the surface finish demanded.

Precision microscopes are devices used with a magnification of around X500 and measure to an accuracy of $+0.5 \mu\text{m}$. The contact pressure used was 10N (100g) within 30 s. Prior to the test, the samples were grounded and polished with sand paper grit 180, 240, 320, 600, 800, 1000, and 1200 successively, and were finally polished on an ultrasonic cleaner. The average results of five best repeated test results out of 10 obtained from the hardness test are presented in **Table 4**. The relationship between hardness, temperature of the specimens obtained from the hardness tests, are presented in **Figure 15** (specimen heat treated at 850°C exhibited poor hardness), whereas, the materials at 900 and 950 show effective resistance to indentation.

3.2. Tribological behaviors

In many cases, lubricants are used to solve tribological problems. But in certain cases, lubrication is not possible: thus where lubrication has to be avoided (for economic or ecological reasons) or when the lubricant cannot be applied at the point at which it is needed (is inaccessible), friction and wear behavior is indispensable under critical operating conditions. Tribology is an important contribution to our prosperity, from daily life to advances in technology. Tribological research work and tribotesting achieve these important goals by:

- decreasing pollution and saving the environment
- decreasing energy losses
- preserving raw materials

Considering these in perspective, the aims of tribotesting can be specified as follows:

- To add to general tribological knowledge, with a better understanding of mechanisms as a basis for specific developments.
- The tribological characterization of improved or new materials to define their areas of application.
- The solution of real tribological problems, improvement of functionality or life by modification of materials, construction or running circumstances.

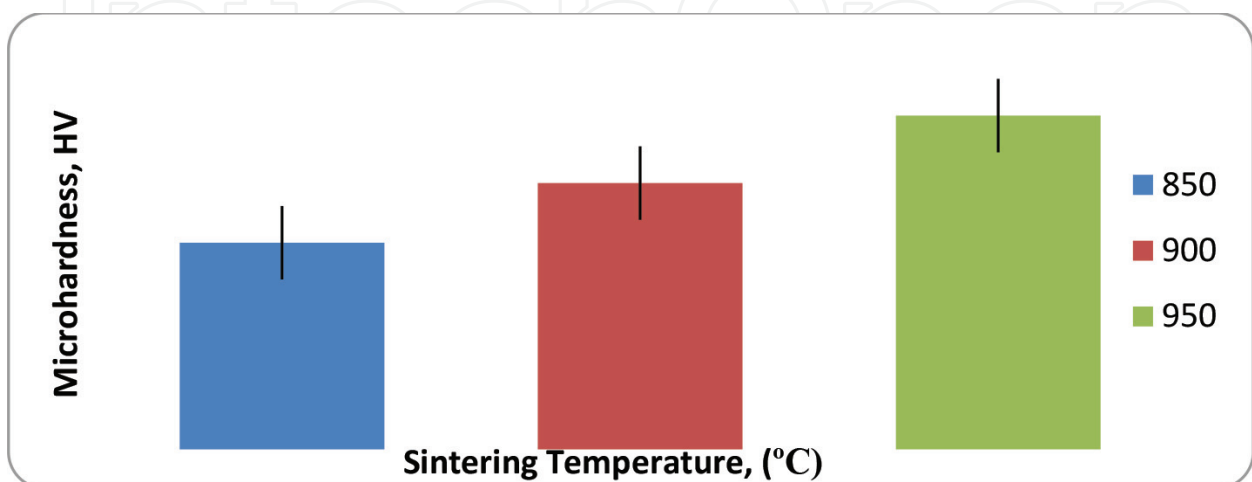


Figure 15. Relationship between hardness and sintering temperature.

Microstructure refers to the microscopic description of the individual constituents of the physical substances used as inputs to manufacturing. It is necessary to examine these individual constituents and their influence on the tribological properties of the materials. Microstructure, which basically refers to grain size and shape and other microstructural characteristics, goes a long way in influencing the mechanical and wear behavior of a material. Optical, electron, and scanning probe microscopes are commonly used in microscopy. These instruments aid the examinations of the microstructural features of all types of materials. Microscope investigation is very important tool in the study and characterization of materials. Following are some critical applications of microstructural examinations: to predict the properties of materials once these relationships have been established; to ensure that the associations between the properties and structure (and defects) are properly understood; to design alloys with new property combinations; to find whether or not a material has been correctly heat treated; and to ascertain the mode of mechanical behavior. The samples were cut and grounded to shape after sintering and oil dipping. The surfaces of the specimens were first polished with sand papers of grit 180, 240, 320, 600, 800, 1000, and 1200 successively, and then polished in two stages using 3 μm and 0.05 μm , respectively. The purpose of this study was to examine the distributions of the alloy particles in copper-based matrices and to also help evaluate the porosity and the density. The specimens were then etched with a solution 3% hydrogen peroxide (H_2O_2). Each specimen was immersed in the etchant solution, followed by immediate rinsing under running water and then alcohol rinsing, thereafter. Finally, the specimen was hand dried carefully for optical microstructure analysis. The scanning electron microscopes (SEM) were also employed to examine microstructures of the specimen before and after the tribotest. Before the SEM analysis, the samples were immersed in a cylinder containing Ethanol absolute for ultrasound cleaning in a Honda W-113 Ultrasound multi cleaner for 40 min in all however changes the ethanol absolute liquid every 10 min. The SEM equipment used was S-3700N SEM-HITACHI. The energy dispersive spectroscopy (EDS) analysis was also conducted on some particular selected zones of the samples. The QUANTAX 400-EDS was also used.

Figure 16 shows the typical SEM microstructures of compacts sintered at a constant pressure and at temperatures 850, 900, and 950°C, respectively.

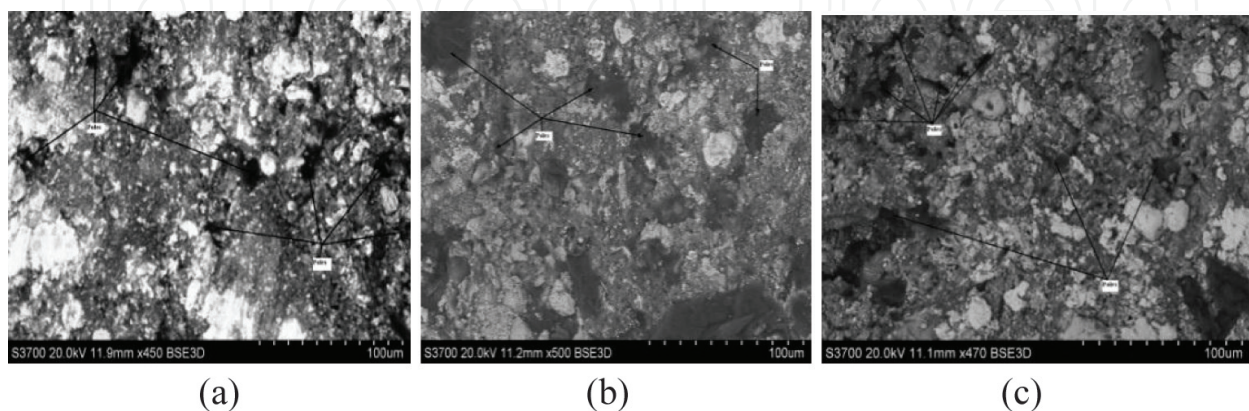


Figure 16. SEM micrograph before tribotest: (a) 850°C, (b) 900°C, and (c) 950°C.

The microstructure shown in **Figure 16(a)** of the test samples shows an irregular copper matrix, with fine graphite powder stored in the pores (the black spots). This could be seen almost in all the samples but the fraction is not the same therefore resulting in a different response to wear behavior.

Figure 17 shows the nature of the OM before the braking test. The dark spot found here confirms the volume of pores on the surface under examination and the influence of it on the overall performance of the novel material when subjected to braking application. Compared with the SEM, it is quite obvious that adequate porosity can be achieved to help produce more effective material for train brake pads. These pores are as the result of graphite and other low melting alloys trapped in the voids. This eventually serves as fuel to lubricate the dry sliding process.

The typical variation of coefficient of friction, wear coefficient, and the wear number obtained during the dry sliding tests conducted on the X-MSM Constant Speed Friction Material Tester at the applied constant pressure of 3.13 MPa is shown in **Table 5** for the materials investigated.

Figure 18(a) shows the relationship of the coefficient of friction and the sintering temperature. The coefficient and the disk operating temperature graphs are also shown in **Figure 18(b)**, which shows that, at the start of the test, the coefficient was high for all the samples, but exhibited a little reduction as it kept increasing in revolution. The average rate of reduction was recorded at 0.0186, 0.0162, and 0.0052 for all the materials investigated at a temperature of 850, 900, and 950°C, respectively.

The wear behavior phenomenon of the material at different sintering temperatures was critically surveyed. The volume loss during the tribotest at various disk operating temperatures was compared to the mathematical evaluations of the volume loss and the results are shown in **Table 6**. The pin-on-disk tribotester method was used, to relate the volume loss with the porosity of the material at different sintering temperatures bearing in mind the operating conditions. **Figure 19(a)** shows the varied relationship between the wear number and the wear coefficient at the same sintering temperatures. **Figure 19(b)** shows the relationship developed between the wear number and the porosity at sintering temperatures. The relationship between the wear number and the wear coefficient at disk operating temperatures is also shown in **Figure 19(c)**. The behavior of the coefficient of friction and the hardness at sintering temperature is shown in

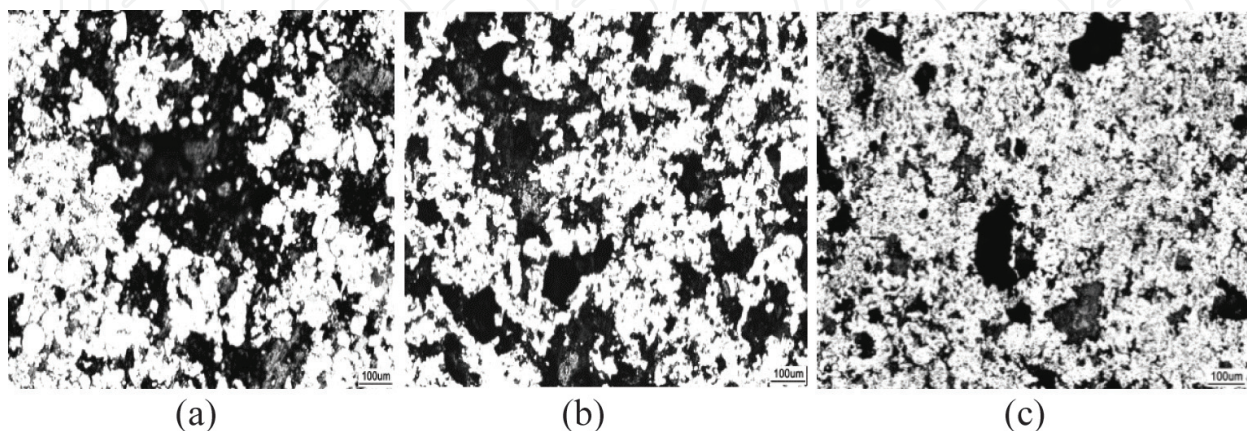


Figure 17. OM micrograph before tribotest: (a) 850°C, (b) 900°C, and (c) 950°C.

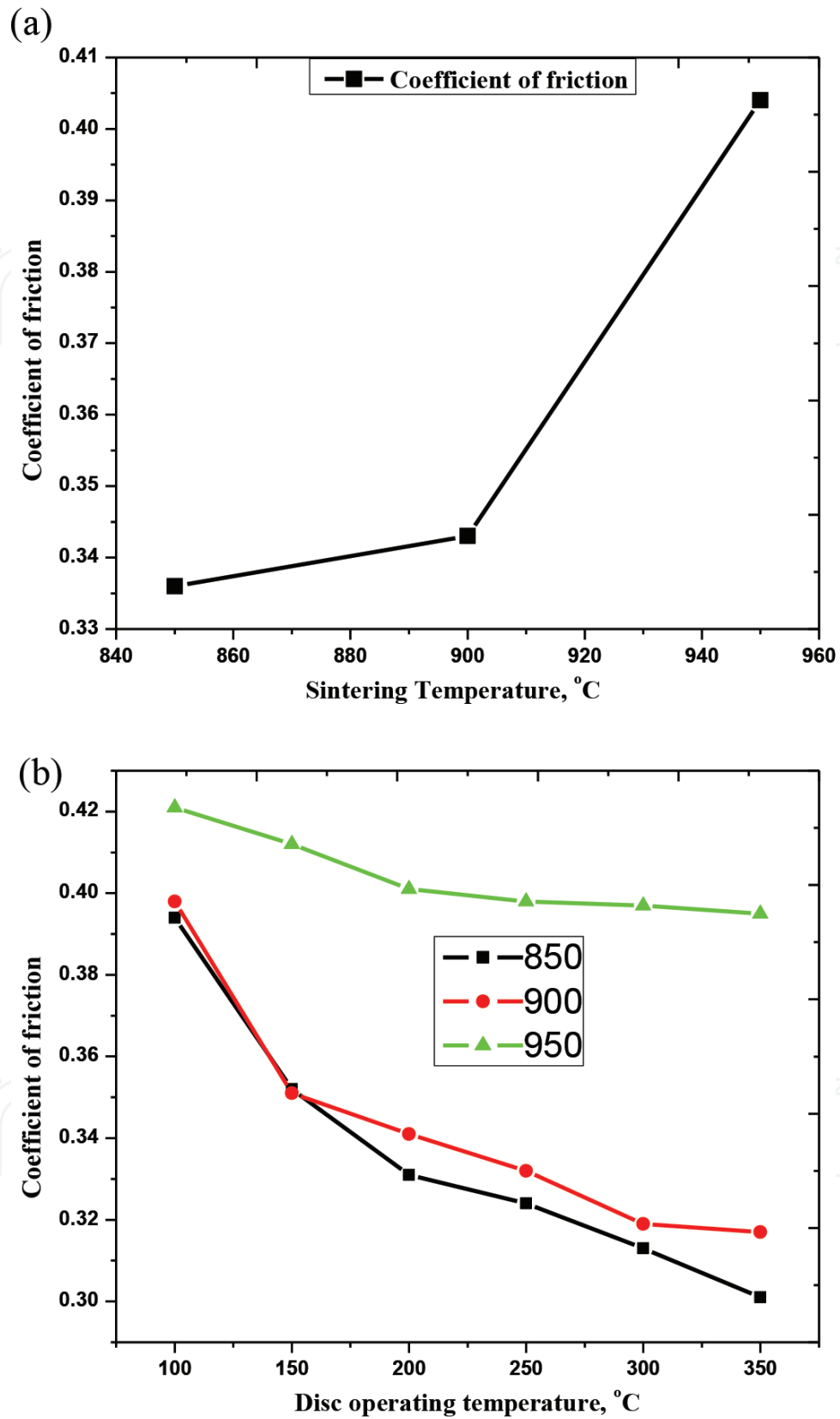


Figure 18. Coefficient of friction as a function of (a) the sintering temperatures and (b) disk operating temperatures.

T_{sin} °C	Disk temperature (T_{disk})						
	Volume	100°C	150°C	200°C	250°C	300°C	350°C
850°C	V_p	0.512	0.515	0.517	0.519	0.521	0.522
	V_t	0.737	0.742	0.745	0.748	0.751	0.752
900°C	V_p	0.679	0.681	0.685	0.687	0.689	0.691
	V_t	0.927	0.930	0.936	0.938	0.941	0.943
950°C	V_p	0.213	0.257	0.287	0.291	0.301	0.308
	V_t	0.275	0.331	0.370	0.375	0.388	0.397

NB: V_p and V_t are all in mm^3 .

Table 6. Comparing the volume loss (theoretical and practical).

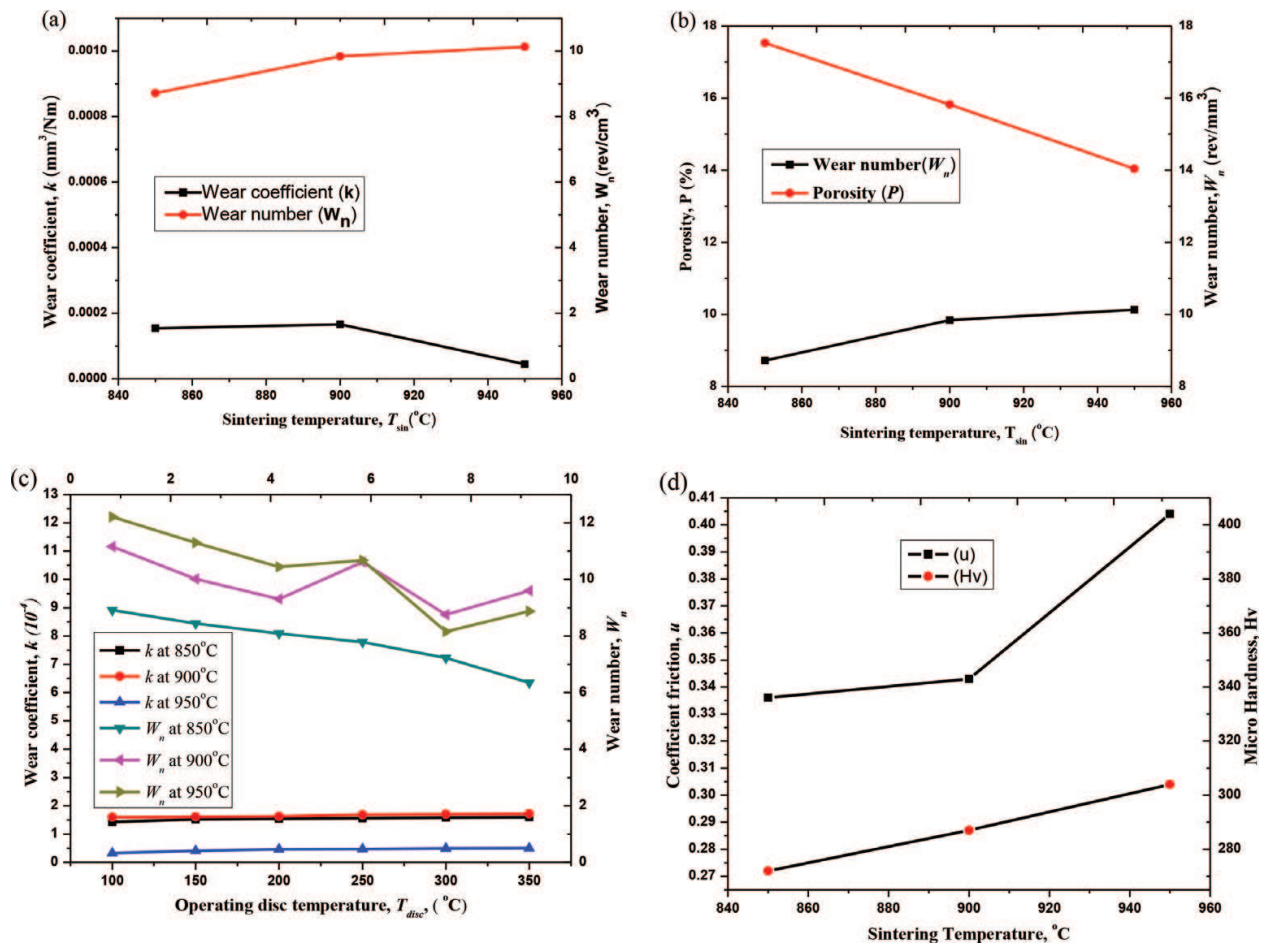


Figure 19. Tribological behaviors varying with temperatures. (a) Variation of wear number and wear coefficient as a function of sintering temperatures; (b) variation of wear number and the porosity as a function of sintering temperatures; (c) the wear number, the wear coefficient as a function of the disk operating temperature; (d) the μ , and H_v as a function of sintering temperatures; (e) the H_v and W_n as a function of sintering temperatures.

Figure 19(d). Finally, the variation of the wear coefficient and the microhardness at sintering temperatures is also shown in (e).

The mathematical expression of the volume loss used to compare with the derived one from the experiment is shown as follows;

$$V = \frac{kPL}{H} \quad (25)$$

where H is the hardness of specimen, V is the volume loss, P the applied load, L the sliding distance, and k the wear coefficient. The equation shows that the volume loss of a material is inversely proportional to its hardness. Therefore, the higher the reinforcement elements in content, the better wear resistance and reduction rate of volume loss.

The wear mechanisms of the sintered Cu-based composite rubbing against a rotor, the disk made of cast iron (grade HTA5/HB with Brinell hardness in the range 196), the worn surfaces of the composite specimen and wear debris were examined by SEM. The typical SEM microphotograph of the worn surface for novel Cu-based composite containing 17.53% porosity and sintered at 850°C is shown in **Figure 20(a)**. The exerted braking pressure is 3.13 MPa and the constant sliding speed of 7.4 m s⁻¹.

The use of X-rays are electromagnetic radiation of wavelength about 1 Å (10⁻¹⁰ m), which is about the same size as an atom. They occur in that portion of the electromagnetic spectrum between gamma-rays and the ultraviolet rays. X-ray diffraction is one of the most important characterization tools used in solid state chemistry and materials science, therefore it is used here to determine the size and the shape of the unit constituents in the composition of the material.

Figure 21(a–c) shows the XRD pattern of the worn surface of material at sintered temperatures of 850, 900, and 950°C, respectively.

The electrons interact with the atoms that make up the sample producing signals that contain information about the sample's surface topography, composition and other properties.

The typical SEM microphotographs of the worn surface for novel Cu-based composite after undergoing a successful braking process are shown in **Figure 22**. These micrographs are

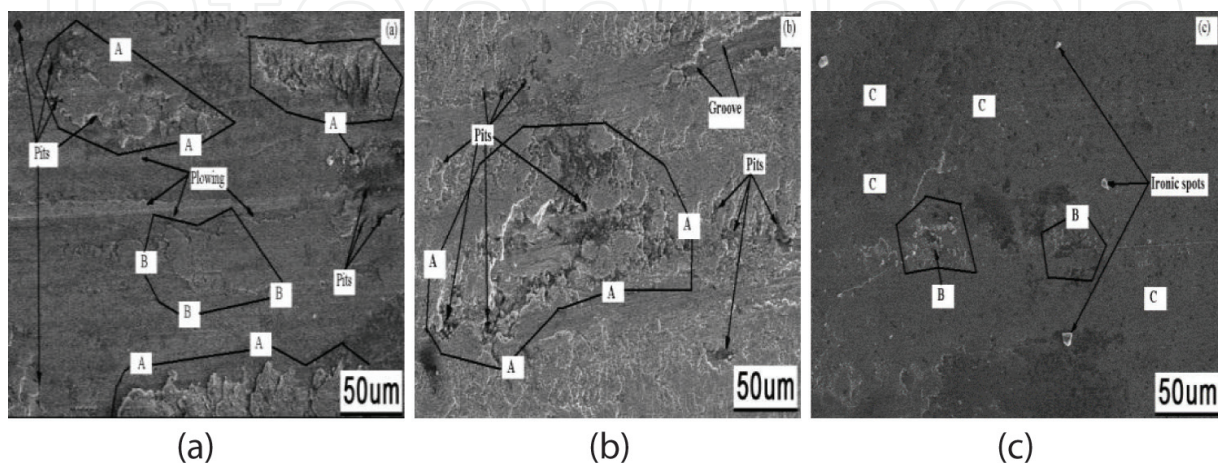


Figure 20. SEM micrograph of friction surfaces at: (a) 850°C, (b) 900°C, and (c) 950°C.

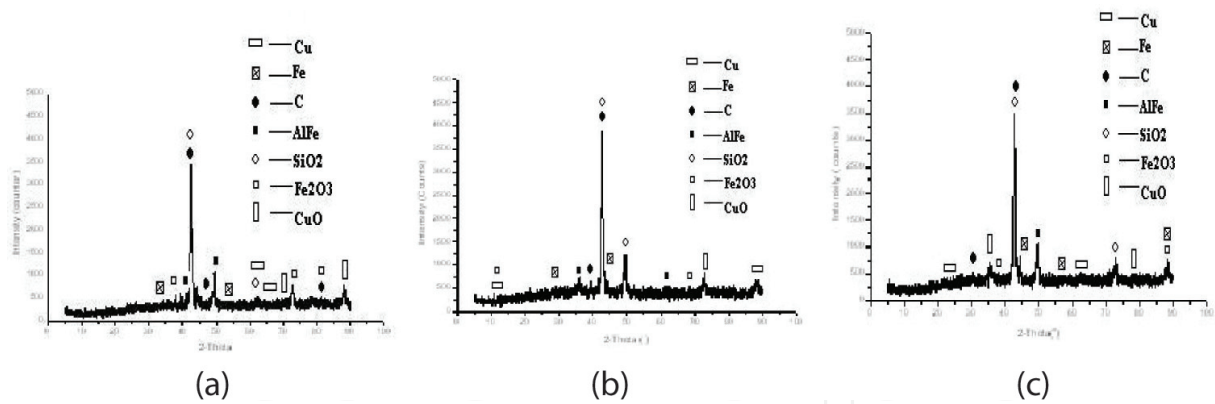


Figure 21. XRD of worn surface at sintering temperatures at: (a) 850°C, (b) 900°C, and (c) 950°C.

typically the nature of the novel material under the SEM microscopy. Sample (a) sintered at 850°C; (b) sintered at 900°C; (c) sintered at 950°C shows worn surfaces of various degrees after successful braking application.

The image processing and computer-based world have generated an automated tribological surface. These generated surfaces are quality control during manufacturing, wear failure analysis of engineering components, and wear particles monitoring in machine condition. **Figure 23** shows 3D Talysurf shaped images of the hybrid fractal-wavelet; they are of three classes of abrasive surfaces as indicated by reference [31].

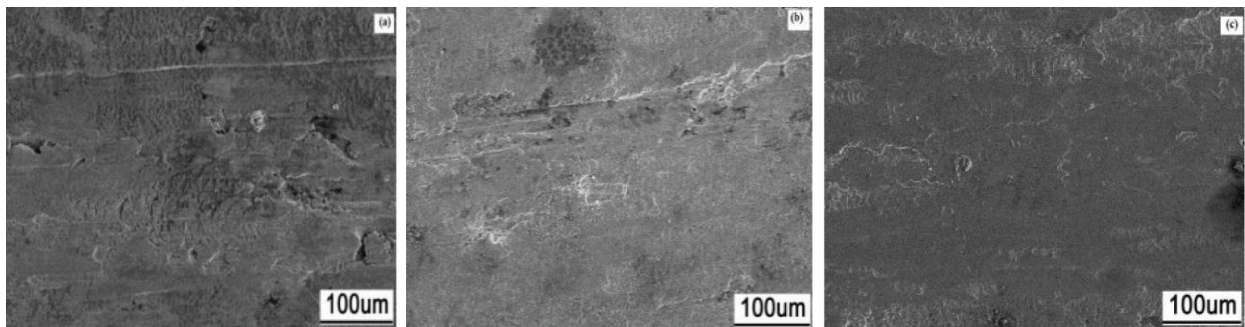


Figure 22. SEM micrographs of the worn surface for Cu-based composite.

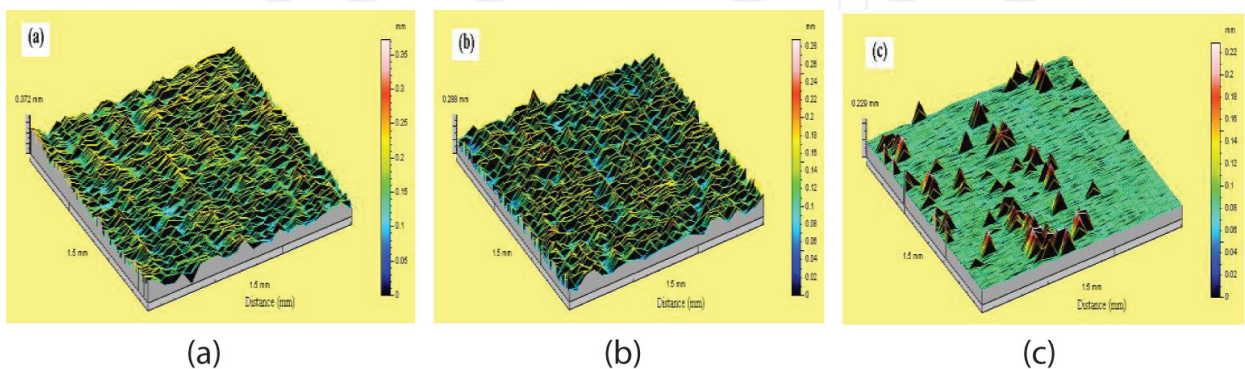


Figure 23. 3D Talysurf images of the surface at: (a) 850°C, (b) 900°C, and (c) 950°C.

4. Results analysis

4.1. Mechanical behaviors

The average apparent density for the novel composite material was 6.7136 g/cm^3 . The ROM calculated density value of the same material was 7.973 g/cm^3 as shown in **Table 3**. The apparent density for the novel material was lower than the theoretical, therefore reducing brake weight and lowering total material usage and improving brake surface. The results generated an average porosity of 15.79% in the composite as the discrepancy between the experimental data and the calculated result, which is within the acceptable range (10–35%) of porosity in PM materials. This is illustrated in **Figure 14(a)** and **(b)**. The sintering temperature of 950°C of the specimen produced a remarkable porosity reduction and a better densification. These were as a result of the reduction and elimination of pores in Fe particles primarily bring about the densification of the composite. It can further be ascertained that a high sintering temperature promotes the sintering driving force and self-diffusion and interdiffusion of atoms.

At higher sintering temperatures, better mechanical properties of the material were achieved. A favorable porosity of 14.4% of the novel composite material was within the acceptable porosity of 15% of a composite PM material for dry sliding friction required to serve as self-lubrication property of the novel material which helps prevent seizure. Also, adequate internal porosity enhances brake formulations by reducing brake weight and lowering total material usage as well as improving brake surface. **Figure 14(a)** and **(b)** shows that the novel material has the potential of being able to maintain effective friction material for high speed train brake pads, particularly the sample sintered at 950°C . Therefore, sintering temperature in this case influences the porosity and improves the density of the material.

In this investigation, the material's ability to withstand wear and indentation or scratches is well associated with the degree of hardness (hardenability). In **Figure 15**, the results show that the highest hardness of the novel material was achieved at the maximum sintering temperature (950°C). Within the same sintered material, a good wear resistance of the material is also observed in **Figure 19(c)**. This result evidenced decreases in the wear rate and high wear number of the novel material indicating high resistance to wear of the sliding pair (ASTM B611). It can also be observed in **Figure 18(a)** that there is a relationship between the coefficient of friction and the hardness since the highest sintered novel material also exhibits the highest coefficient of friction.

The graph in **Figure 15** also indicates that the hardness is proportional to the sintering temperature. This can be attributed to the fact that high sintering temperature promotes complete diffusion of both self and inter of the atoms. Information can also be observed in **Tables 3** and **4**, which contains some of the physical and mechanical properties of the novel material.

4.2. Tribological behavior

The phenomenon here is very simple when you look at both surfaces of the SEM and OM shown in **Figures 16** and **17** before the braking process. The surface characteristic shows dark spots on both micrographs, therefore, indicating that the degree of porosity could be high. This

enables the needed pores for effective dry sliding operation except when novel materials with incomplete diffusion particularly 850°C and 900°C are not able to demonstrate better resistance to wear as shown in **Figure 19(a–e)**.

At high porosity, the self-lubrication property becomes high and reduces seizure. Many large pores are exposed in the frictional process. These pores may collect the debris, usually oxides. The collected oxides not only increase the real contact area between the pin and disk but also act as a solid lubricant source when the nonporous areas have metallic contacts with the disk. In this case, the high porosity sintered specimens have relatively low frictional-coefficients because oxides always exist on the contact area even in the case of metal-metal contact. These oxides and the wear debris plow or cut the specimen surface as abrasives or the disk surface when found inserted in the surface pores. When these specimens are in dry sliding operation, the main contact areas become smaller for high mass loss samples, and the high contact pressure makes thin contact areas between pores easily worn off. However, the sintered specimen with high porosity yielded high volume loss and those with low porosity yielded low volume loss.

It can be seen in **Figure 18(a)** that the entire sintered specimen saw a decline from the highest to the lowest frictional coefficient at the increase of the disk operating temperature. The specimen with the highest porosity was observed at a low sintered temperature, which contains an extremely low frictional coefficient. This indicates that the sintering treatment temperature influenced the frictional coefficient under the given wear test condition. In this case, it was observed that, the higher the sintering temperature gives a better coefficient friction, which confirms the fact that, the minimum porosity expected to reduce the rate of wear was obtained at a high sintering temperature. When porosity was formed in the material, a low coefficient of friction was observed, mostly at the lower sintering temperatures.

The wear number and the wear coefficient variation with operating disk temperatures for sintered specimen at 850, 900, and 950°C with different porosity are plotted in **Figure 19(c)**. The sintered specimens with high porosity (850 and 900°C) have a high volume loss. This is confirmed by the values obtained as the wear coefficient and the wear number, which contain low and high values for the one with low porosity (950°C) and also contain low volume loss at constant pressure and sliding speed (3.13 MPa and 7.5 ms⁻¹) under which the machine was operating. This indicates that during the entire sliding wear testing, the volume loss of the sintered specimen decreases with a decrease of porosity, which is observed as a result of the sintering temperature.

The specimens with higher porosity have higher volume loss and the one with the lower porosity has lower volume loss. The specimens with the higher porosity also are those sintered at low sintering temperature and those with lower porosity were sintered at high sintering temperature. From the above experimental results, it can be concluded that the volume loss and wear coefficient of sintered Cu-based composite increase with the increase of sintering temperature, thereby increasing the porosity of the composite.

The influence of the sintering temperature on porosity affects the volume loss and can be linked to the wear number and the wear coefficient, which is illustrated in **Table 5** and can be

seen in **Figure 19(c)**. The samples with high wear numbers were noted to be those with low porosity and therefore have low volume loss. On the other hand, those with low porosity have low wear numbers and high volume loss. The low wear coefficient was seen to also have low porosity and high wear coefficient contains high porosity, therefore resulting in high volume loss and low volume loss, respectively. The wear mechanisms of the sintered Cu-based composite rubbing against a rotor, the disk made of cast iron (grade HTA5/HB with Brinell hardness in the range 196), the worn surfaces of the composite specimen and wear debris were examined by SEM. The typical SEM microphotograph of the worn surface of the novel Cu-based composite that contained 17.53% porosity and was sintered at 850°C is shown in **Figure 20(a)**. The exerted pressure was 3.13 MPa and the sliding speed was 7.4 m/s. The worn surface appears to contain some small fine grooves of wear tracks and break-away abrasive kinds of wear.

Figure 20(b) shows the SEM microphotograph of the worn surface for the novel Cu-based composite containing 15.82% porosity, sintered at 900°C resulting from dry sliding against the same cast iron rotor at constant pressure and sliding speed as mentioned above. The presence of high pores in both micrographs before wear test have led to some portions of the specimen to appear with flake-like fragments containing initiation and propagation of subsurface cracks. The intensity of the pressure was also observed as part of the problem. In addition, some pits or cavities could be observed on the specimen's surface due to stress induced by high pressure. The delamination wear was observed. This can be attributed to insufficient heat causing the necessary diffusion. In this case, the porosity becomes affected, which eventually affects the densification as well.

Figure 20(c) shows material containing 14.04% porosity tested under the same conditions as the previous two samples. There are a few iron particles feasible on the surface. The micrograph shows a very smooth surface with these iron spots that turn to reduce the area of contact between the disk and the specimen, therefore reducing the rate of wear. Generally, the friction's firm destruction observed are grouped into three sections; namely, intense wear very rough surface, medium wear-relatively smooth surface and smooth surface-mirror like surface. The A sections on the photograph indicate intense wear sections. B sections show relatively rough wear and section C representing a mirror-like surface, a better wear resistance surface. Here, the samples were assumed to have had sufficient heating during the sintering operation, therefore, showing less destruction of the tested surface.

The groove (in **Figure 20a**) reveals plowing that occurred during sliding. The novel Cu-based composites are composed of several elements with different wear resistance properties. The elements with hard particles have better wear resistance than the soft elements. Therefore, hard particles projected on the friction surface; whereby the relative motion between composite and counterpart is prevented, turn to produce a higher coefficient of friction than the soft ones. At the same time, the hard particles projected turn to reduce the area of contact between the friction surfaces in contact thereby reducing the rate of wear. These high porosity specimens are known to have fewer hard particles than low porosity specimens. The high porosity sintered composites have more interconnected pores and fewer hard particles. These exhibit lower strength, are much easier to deform and are easily torn off, especially at the start of the

wear process. Therefore, high porosity samples have a low coefficient of friction, low wear number and high wear coefficient resulting in high volume loss as shown in **Table 5**. There were shallow and deep pits on the surface of high porosity Cu-based composites (a and b). This is a result of inherent pores, which are on the surface of sintered specimens or were discovered when the material above was worn away during the tribo test. At lower porosity, the size and number of pits is minimized. This is caused mainly by the surface fatigue (**Figure 20a**), i.e., where delamination wear occurred. Also abrasive wear occurred as the result of using wear debris as an abrasive for plowing both the oxide layer and metallic area. From the discussions above, the wear mechanisms of Cu-based train brake composites underwent plowing wear, delamination wear and abrasive wear. Any of these can lead to severe destruction of the worn surface and result in excessive wear, rough braking, and even failure in braking.

Figure 21(a–c) shows the XRD pattern of the worn surface at sintering temperatures of 850, 900, and 950°C, respectively. The worn surface depicts the pattern that the main components of the worn surface are graphite, SO₂, Fe, Cu, and oxides of Fe and Cu (Fe₂O₃ and CuO) and AlFe. Graphite has a layer structure with wider interlayer spacing, which tends to cleave along the layers. So it is widely used as lubricant to eliminate seizure and make the brake process stable. Consequently, the tribological properties of brake materials are improved [32]. The resistance and hardness of SiO₂ and CuO particles are much higher than those of the Cu and Fe matrix due to particulate hardening. Therefore, the friction coefficient is improved remarkably as a result of friction of SiO₂ against counterpart and this is intense during sliding, which hinders the relative movement of friction pairs yielding a high friction coefficient.

The typical SEM microphotographs of the worn surface for Cu-based composites are shown in **Figure 22**. The (a) sintered at 850°C shows that the worn surface appears to contain some small fine grooves and break-away abrasive kind of wear. The groove in **Figure 22(a)** reveals that plowing occurred during sliding. The (b) sintered at 900°C shows flake-like fragment, initiation, and propagation of subsurface cracks. Some pits or cavities can be observed at the specimen's surface due to stress caused by high pressure or load during operation. Delamination wear was exhibited which was attributed to insufficient heat to cause necessary diffusion. In c, sintered at 950°C, there are a few iron particles feasible on the surface. The micrograph shows a very smooth surface with these iron spots that turn to reduce the area of contact between the disk and the specimen, therefore reducing the rate of wear. Generally, the worn surfaces observed are grouped into three sections, namely destructive wear section (found mostly on (a) and (b)), medium wear section (mostly on (a) and very small area on (c)), and low wear section (only on (c)).

The Cu-based composites are composed of several elements with different wear resistance properties. The elements with hard particles have more substantial wear resistance than the softer elements. Therefore, the hard particles projected on the friction surface; whereby the relative motion between composite and counterpart is prevented, turn to produce a higher coefficient of friction than the soft ones. At the same time, the hard particles projected turn to reduce the area of contact between the friction surfaces in contact thereby reducing the rate of wear.

In **Figure 23**, our investigation generated abrasive surfaces classified into the following sections: smooth surface due to minimal wear rate and better wear resistance property, rough surface because of moderate wear rate, and highly rough surface due to excessive wear. The 3D Talysurf images of the surfaces are shown in **Figure 23**. **Figure 23(a)** shows a highly rough abrasive surface; it has fewer peaks that are ironic to withstand pressure from the braking system. **Figure 23(b)** represents the rough abrasive surface with moderate peaks withstanding the exerted pressure of the braking system. The (c) is the one that was observed as having enough ironic peaks to withstand the exerted pressure and therefore given a smooth abrasive surface.

5. Conclusions

According to this research, the following conclusions were made on the mechanical and tribological characteristics during the sliding wear behavior of novel Cu-based composite material against a cast iron (grade HTA5/HB with Brinell hardness in the range of 196).

- Generally, tribological behavior of all the sample material is temperature sensitive such that the transition from severe wear which initiates at lower temperatures (850 and 900°C) reduces as the temperature increases during high sintering temperature (950°C). This means the samples sintered at low temperatures suffer severe wear but at high temperatures low wear was calculated and practically recorded as well.
- As porosity was reduced, densification of the material was also improved indicating the reduction and elimination of pores in Fe particles to improve densification of the composite. Furthermore, high sintering temperature promotes the sintering impetus, the self-diffusion, and interdiffusion of atoms that are improved to accelerate the densification. Also graphite entrapped in the pores then leads to strengthening the densification of the composites to a certain degree.
- The dominant wear mechanisms observed were plowing, delamination, and abrasive wear. High porosity samples were affected by delamination and plowing wear. Many pits and grooves were observed. Large flakes were also observed due to the intense nature of the delamination wear. Abrasive wear and delamination wear were the main cause of high wear coefficient, low wear number and low coefficient of friction. This was dominant in high porosity samples. Intense wear and mild wear were feasible in the high porosity samples. Low porosity samples endured less mild wear and showed a mirror-like surface, glassy luster, and integrated friction film. This gives evidence that this section has better wear resistance property.
- The friction coefficient at high sintering temperature with high values indicating firm gripping at stopping at the same time demonstrated low rate of wear. This can be improved further and considered for manufacturing commercial brake pads. The main components of worn surfaces are graphite, SO₂, Fe, Cu, and oxides of Fe and Cu (Fe₂O₃ and CuO) and AlFe. The worn surfaces were divided into three sections: destructive wear section, medium wear section and low wear section. This is due to the level of destruction of friction film during dry sliding.

- The characteristics of abrasive surfaces generated were into three categories, namely smooth surface, which shows minimal wear rate; the rough surface, which depicts temperate wear rate; and the highly rough surface showing extreme wear with a high degree of surface destruction.
- The volumetric and wear coefficient progresses greatly with the increase in sintering temperature. The wear coefficient (k) and the coefficient of friction were generated mathematically as shown in Ref. [28].

Sintering temperature affects the porosity and advances the density of the material. This eventually affects the hardness of the material which decreases the volumetric wear rate and yields a high wear number of the novel material, indicating high resistance to wear of the sliding pair. Further increase of sintering temperature greatly affects microstructures and tribological characteristics of Cu-based friction materials. It is clear that further studies of this material can improve the manufacturing of commercial brake pads [28].

Acknowledgements

This work was supported by the National Natural Science Foundation of China (Grant Nos.: 51575190, 51675105 and 51575113) and China Post-Doctoral Fund (Grant No: 2015M582357).

Author details

Glenn Kwabena Gyimah^{1*}, Zhongning Guo¹, Ping Huang² and Dong Chen²

*Address all correspondence to: gk.gyimah@yahoo.com

1 Faculty of Electromechanical Engineering, Guangdong University of Technology, Guangzhou, China

2 School of Mechanical and Automotive Engineering, South China University of Technology, Guangzhou, China

References

- [1] Savage, G., Applications of Carbon-Carbon composites. Carbon-Carbon Composites, first ed., Chapman & Hall, London, 1993, pp. 323–346.
- [2] Hasegawa, I., Uchida, S, "Braking Systems," - Japan Railway Technology Today (Edited by Kanji Wako), Japan, June, 1999.
- [3] Nicholson, G., (1995) Facts About Friction, P &W Price Enterprises, Inc., Croydon, PA.

- [4] Tatarzicki, Y.T. and Webb, R. T., Friction and Wear of Aircraft Brakes, ASM Handbook, Vol. 18ASM International, Materials Park, Ohio, 1992, pp. 582–587.
- [5] Spurr R. T., (1972) “Fillers in Friction Materials” *Wear*, 22, pp. 367-409.
- [6] Anderson A. E., “Wear of Brake Materials” in *Wear Control Handbook* (edited by M.B. Peterson and W.O. Winer), ASME, New York, USA, 1980, pp. 843–857.
- [7] Hutchings, I. M., *Wear – Materials, Mechanisms and Practice* (Edited by Gwidon W. Stachowiak), November, 2005, John Willey & Sons, Ltd, Chichester.
- [8] Almen, J. O., in *Mechanical Wear* (ed. J. T. Burwell) American Society of Metals, 1950, pp. 229–288.
- [9] Glossary of terms and definition in the field of friction, wear and lubrication, research group on wear of Engineering Materials, organization for Economic co-operation and development, 1969, reprinted in *wear control Handbook* (edited by M. B. Peterson and W. O. Winner), American society of mechanical engineers, New York, 1980, pp. 1143–1303.
- [10] Standard terminology relating to wear and erosion, standard G-40-01, American Society for Testing and Materials, 2001.
- [11] Kato, K., Classification of wear mechanisms in wear—mechanisms, materials and practice (ed. G.W. Stachowiak). John Wiley & Sons Ltd, Chichester, 2006 pp. 9–20.
- [12] Fischer, T. E. and Sexton, M. D. The tribochemistry of oxidative wear in physical chemistry of the solid state. Applications of metals and their compounds (ed. P. Lacombe) Elsevier, Amsterdam, 1984. pp. 97–107.
- [13] Fischer, T. E. and Mullins, W. M. Chemical aspects of ceramic tribology, *The Journal of Physical Chemistry*, 96, 1992, 5690–5701.
- [14] Gates, R. S., Hsu, S. M. and Klaus, E. E. The tribochemistry mechanism of alumina with water, *tribology transactions*, STLE 32(3) 1989, 357–363.
- [15] Lim, S. C. and Ashby, M. F., *Wear Mechanism map*, *Acta Metallurgica*, 35, 1987, 1–25.
- [16] Adachi, K., Kato, K. and Chen, N., *Wear Map of ceramics*, *Wear* 203–204, 1997, 291–301.
- [17] Zum Gahr, K. H. *Microstructure and Wear of Materials Tribology Series*, Elsevier, Amsterdam, 1987, pp. 132–148.
- [18] Hokkirigawa, K. and Kato, K., Theoretical Estimation of Abrasive Wear Resistance Based on Microscopic Wear Mechanisms *Wear of Materials* (ed. K. C. Ludema), ASME, New York, 1989, pp. 1–8.
- [19] Archard, J. F., Contact and robbing of flat surfaces, *Journal of Applied Physics*, 24, 1953, 981 – 988.
- [20] Rabinowicz, E., *Friction and Wear of Materials*, 2nd edn. Wiley-Interscience, New York, 1995.

- [21] Kapoor, A. and Johnson, K. L. Plastic ratcheting as a mechanism of metallic wear, Proceedings of the Royal Society of London, 445, 1994, 367–381.
- [22] Kapoor, A., Johnson, K. L. and William, J. A. A model for the mild Ratcheting Wear of Metals; Wear, 200, 1996, 38–44.
- [23] Lundkey, G. and Palongrev, A. Dynamic Capacity of Rolling Bearings, Ingeniorsveten – S Kapsademicns, no. 96, 1947.
- [24] Weibull, W. A statistical theory of the strength of materials, Royal Swedish Academy of Engineering Science Proceedings, 151, 1930, 5–45.
- [25] Challen, J. M., Oxley, P. L. B. and Hockenhull, B. S. Prediction of Archard's wear coefficient of metallic sliding friction assuming a low cycle fatigue wear mechanism, Wear, 3, 1986, 275–288.
- [26] Kryachek, V. M. “Sintered Metals and Alloys Friction Composites: Traditions and New Solutions(Review). Powder Materials” Powder Metallurgy and Metal Ceramics, Vol. 43, Nos. 11–12, 2004 Spring Science + Business Media, Inc.
- [27] Yao, P., Sheng, H., Xiong, X., Huang, B. Worn surface characteristics of Cu-based powder metallurgy brake for aircraft, Transactions of Nonferrous Metals Society of China, 17, 2007, 99–103.
- [28] Gyimah, G. K., Chen, D., and Huang, P. Dry Sliding Wear Studies of Cu-Based Powder Metallurgy Brake Materials, Volume 3. Design Materials and Manufacturing Parts A B and C, 2012.
- [29] Xiong, X., Sheng, H., Chen, J., and Yao, P. Effects of sintering pressure and temperature on microstructure and tribological characteristic of Cu-based aircraft brake material, Transactions of Nonferrous Metals Society of China, 17, 2007, 669–675.
- [30] Gyimah, G. K., Huang, P., and Chen, D. “*Dry sliding wear studies of copper-based powder metallurgy brake materials*”, ASME Journal of Tribology, *J. Tribol.* Volume 136, Issue 4, pp. 041601-041606 (May 19, 2014).
- [31] Stachowaik, G. W., Stachowiak, G. B., De Pellegrin, D., Posiadlo, P. Characterization and Classification of Abrasive Particles and Surfaces, Wear–materials, mechanisms and practice. Edited by G. Stachowiak, 2005, pp. 339–368.
- [32] Stachowiak, G. W., Podsiadlo, P. Surface characterization of wear particles, Wear, 1999, 2251229: 1171–1185.

